The 2011 Lorca earthquake slip distribution controlled by groundwater crustal unloading

Pablo J. González[1], Kristy F. Tiampo[1], Mimmo Palano[2], Flavio Cannavó[2] and José Fernández[3]

[1]Department of Earth Sciences, University of Western Ontario, Biological and Geological Sciences Building, London, Ontario N6A 5B7, Canada. [2]Istituto Nazionale di Geofisica e Vulcanologia, Osservatorio Etneo - Sezione di Catania, Piazza Roma, 2, 95123, Catania, Italy. [3]Instituto de Geociencias (CSIC-UCM), Facultad de Ciencias Matemáticas, Plaza de Ciencias 3, Ciudad Universitaria, 28040 Madrid, Spain.

Detailed studies of earthquakes triggered by a known source of stress change can shed light on the influence of fault frictional properties[1,2] and preseismic stress[3,4] on the initiation, propagation and arrest of seismic ruptures. Triggered and induced seismicity can provide unique opportunities to understand this problem[5-7]. However, direct evidence is rare due to the absence of e.g., near-field surface ground deformation observations[8,9] and unknown pre-earthquake stress conditions. Here, we collect geodetic data recording the coseismic effects of the Mw 5.1, 11 May 2011 Lorca (SE Spain) moderate earthquake. Elastic modelling results suggest that the nucleation process and main slip area occurred at very shallow depths (2-4 km) on the rupture plane along the Alhama de Murcia fault. Slip extends towards the surface from unstable to stable friction fault segments. We find that the slip area matches well a pattern of positive Coulomb stress change due to groundwater extraction in a nearby basin aquifer. These results indicate that the shallow slip distribution during the earthquake could be controlled by groundwater induced unloading stresses at the upper frictional transition of the seismogenic layer. The relationship between known crustal stress changes (e.g.,

Nature Geoscience (2012) doi: 10.1038/NGEO1610

groundwater extraction) and coseismic slip distribution could help, in general, to understand where and how earthquakes tend to occur.

The Eastern Betics Shear Zone in South Spain is a transpressive deformation segment of the major diffuse Nubia-Eurasia plate boundary (Fig. 1**a**), where ~NW-SE convergence direction is accommodated in a complex set of thrusting and strike-slip faults[10,11]. This region has suffered a significant number of moderate-to-large earthquakes in the past 500 years and is considered one of the areas of highest seismic risk in Spain[12]. On 11 May 2011 (16:47 UTC), an earthquake struck the city of Lorca (Fig. 1**b**), causing significant property damage, injuring hundreds and resulting in nine fatalities. The epicenter, as determined by the National Geographical Institute of Spain (IGN), was located ~2 km east-northeast of Lorca, with a focal mechanism solution indicative of reverse and strike-slip faulting that occurred at very shallow crustal depths (~3 km)[12]. The mainshock has been tentatively attributed to a major fault in the area, the Alhama de Murcia fault[12] (AMF). Catalogue locations for the entire sequence (~149 events), present an undistinguished pattern[12]; however detailed seismic relocation indicates that most events were generated along the AMF[13] (Fig. 1**b**).

To constrain the coseismic slip, surface deformation was measured by radar interferometry. In addition, available GPS data were processed both at daily and at 1-Hz rates to determine static and transient offsets (see Methods). Two different ENVISAT descending satellite tracks (I2 and I6) imaged the area before and after the event, providing estimates of the displacement field from two different look angles (Fig. 2**a** and 2**c**). Differential interferograms were processed in time series without temporal filtering (see Methods) and resulting displacement maps were corrected for a known groundwater subsidence signal[14] (Fig. 1**c** and 1**d**, and Supplementary Information). Coseismic displacement maps show displacements towards the satellite north of the mapped AMF[11], with deformation peaks at ~2.5 cm (Fig. 2**a**) and ~1.5 cm

(Fig. 2**c**). Deformation reversed south of the AMF, with ~1 cm of displacement away from the satellite (Fig. 2**a** and 2**c**). Finally, deformation in the urban area and south-eastwards with respect to the AMF branch show maximum displacements. All the continuous GPS stations except LORC were stable (Fig. 1**a**, 2**a** and 2**c**). LORC station moved north (4.2±0.8 mm) and slightly to the west (-0.9±0.8 mm), while the vertical motion was not significant. Postseismic deformation can be considered negligible, as evidenced by the absence of transients in the following hours-to-days at LORC (see Supplementary Information).

We model the ground deformation data using an elastic dislocation model[15]. First, we explored for the non-linear dislocation geometry[16], and then solved for the distributed slip. The best-fitting uniform dislocation model indicates a reverse and left-lateral slip fault striking N230E and dipping 70-degrees to NE at very shallow depths (1±0.3 km to 4±0.8 km down dip). Those parameters indicate that the earthquake rupture occurred along the AMF. Those results are in good agreement with seismically derived focal parameters[12]. However, large residuals are found near downtown Lorca (see Supplementary Material). The fault slip distribution was resolved on an extended fault plane (10x10 km^2) with a slightly modified strike to match the asymmetric pattern observed in the interferograms (N225E). The preferred smoothed distributed fault slip model allows for two patches of relative maximum slip. A slip area with mainly oblique motion (reverse and left-lateral, ~15 cm) occurs beneath the La Tercia segment-AMF north of the city of Lorca, at depths ranging from 2 to 5 km, which is consistent with an independent fault slip model estimated using a TerraSAR-X differential interferogram[17]. A much shallower and smaller slip area with left-lateral to pure reverse motion is found beneath the city along the Lorca segment-AMF, ~5 cm (Fig. 3**a**). According to the surface geology, the AMF south-eastern branch has been identified as a vertical or south-dipping thrust, from Totana (~15 km northeast) to Lorca[11,18]. If a small vertical segment (down to 1 km) is introduced in the fault geometry the data fit is improved (Fig. 2**b** and 2**d**). However, this does not significantly modify the slip pattern (see Supplementary Material).

Crustal (un-)loading due to near-surface masses redistribution (water, ice or quarried material) can affect the subsurface stress field altering magma production[19] and seismic activity[20-22]. The Alto Guadalentin basin shows high subsidence rates, >10 cm/yr, due to long-term sustained groundwater pumping[14] (Fig. 1**d**). The subsidence area is bounded by nearby faults (e.g., AMF) and the Guadalentin river (Fig. 1**b**), indicative of possible permeability barriers or structural control in the deposition of compressible sediments. Regional groundwater depletion and related environmental problems have been recognized since the 1960s[23]. While groundwater table level changes are only available at a few wells, Fig. 1**c** shows groundwater depth evolution between ~1960 and 2010, which indicates a drop of at least 250 m. We investigate whether or not the groundwater extraction activity could significantly affect the tectonic fault that was activated during the Lorca earthquake, as the unusual shallow slip may indicate. Here, we calculate the three-dimensional subsurface stress change induced by the crustal load on a homogeneous elastic half-space using the Boussinesq solution[24] and resolve for the Coulomb stress change (ΔCFF) on the fault geometry. We explored a range of possible (unknown) groundwater table change areal shapes, aquifer porosities, the role of pore-pressure diffusion, and fault friction (see Supplementary Information). In Fig. 3**b**, we present ΔCFF resolved along the AMF with a slip rake of 36 degrees, in accordance with the published focal mechanisms. We assume conservative values for the unloading model parameters and a simple aquifer shape based on the aquifer permeability barriers, as these provide a lower bound model for the possible stress changes due to the pumping and permanent groundwater drawdown[23] (see Supplementary Material).

The actual interseismic slip rate and stress/friction conditions on the fault are unknown, which precludes their specific inclusion in the stress model. However, before the 2011 earthquake, the most recent similar, moderate earthquake on the AMF near Lorca occurred in 1818[12]. From paleoseismic estimates for net fault slip (0.07-0.6 mm/yr)[11], the accumulated slip deficit ranges from 1.4 to 12 cm. The upper bound is in good agreement with the estimated maximum coseismic slip magnitude for this event, indicating that the fault had accumulated sufficient interseismic tectonic stress to allow for a similar earthquake rupture, assuming that it had remained fully locked.

Given that the faulting itself was tectonically driven, the pattern of unloading stress changes due to the anthropogenic groundwater changes coincides to a remarkable degree with the areas of significant coseismic slip (Fig 3**a** and 3**b**). Assuming that the hypocentral location coincides with rupture nucleation, slip begins north and outwards of the unloaded aquifer area with a left-lateral to reverse slip component at depths consistent with the maximum values of ΔCFF (Fig. 3**c**) for left-lateral to oblique slip motions due to the relative increase of shear stress change at this region. The ΔCFF model also favours propagation towards the surface laterally along the fault-bounded aquifer as thrust rupture. All studied models predict an increase in ΔCFF towards the surface. This propagation pattern also is supported by analysis of radiated seismic energy directivities[13,25], which are consistent with a predominantly SW and towards-the-surface rupture. However, ΔCFF decreases to smaller values for left-lateral slip rake beneath the unloading and far from the aquifer border (Fig. 3**b**), whereas thrust motion increases due to shallow induced extension (reduction of normal stresses) at depths of 1 km or less (Fig. 3**d**). Conversely, the unloading model also explains the slip arrest, as the slip turns and is dominated by a reverse slip component southwest of the city (Fig. 3**a**). Slip propagation ultimately is limited by the earth surface boundary and the low values of pre-stress for encouraging left-lateral ruptures motion along a parallel outward dipping fault at the same location (Fig. 3). The arrest of the coseismic slip propagation in this location also coincides with the intense shaking and damage in the southwestern part of Lorca (Barrio de La Viña).

Based on established studies of fault mechanics[26], depth-dependent fault frictional change and reduced stresses close to the surface prevent surface coseismic slip[2,5]. These limit the maximum slip area during seismic rupture, inferred from geodetic and seismic data to occur at middle crustal depths of 3-8 km[5]. The inferred slip depth here may indicate that the rupture nucleated at the transition zone between velocity-weakening and velocity-strengthening zones (Fig. 3**c**). The fault slip propagation towards the surface and into the velocity-strengthening area would require that anomalously high-dynamic stresses develop at the crack tip and/or a thick fault gouge[26]. Although the shallow slip area could be an early afterslip effect, it would be limited to the first fifteen days following the earthquake, in accordance with the radar data (Fig. 2**a** and 2**c**). Again, LORC GPS station shows no evidence of postseismic motion. We favour shallow coseismic slip based on the interpretation that the high stress conditions required to propagate coseismic slip into the shallow velocity-strengthening volume likely were in place before the event, as a consequence of the cumulative long-term unloading stress change and the relative position of the fault with respect to the depleted aquifer (mainly shallow extension parallel to the unloading source and left-lateral shear at the aquifer edge boundary). It has been shown that three-dimensional crustal (un-)loading processes can promote long-term fault slip or modulate seismicity beneath the (un-)loading source[20,27,28] and on the periphery[22,29]. Here we present observations and modelling results for a possible link between the crustal unloading and the slip pattern during a single earthquake.

We conclude that the presented data and modelling results are consistent with a groundwater crustal unloading process, providing a reasonable explanation for the observed fault slip pattern, as well the propagation and arrest of fault slip during the earthquake into the shallow crustal velocity-strengthening fault zone. This study reveals an unexpected human-induced alteration of the ambient subsurface stress field close to an active seismogenic source, and provides insights into processes that could modify the seismic hazard analysis and elsewhere.

Methods

We correct the differential interferograms for orbital trends by adjusting a bilinear function in a least squares sense. We estimated the bilinear model using the entire interferogram. Masking the deformation area has a negligible effect. We estimated for the displacement time series and associated errors using a multitemporal InSAR time series method (see Supplementary Material). It takes into account decorrelation, individual atmospheric noise, and observations redundancy from a Monte Carlo estimation process[30]. Interferogram atmospheric noise was estimated fitting a 1D zero-order Bessel and exponential covariance function based on randomly distributed points, but excluding points in the deformation region. The final displacement maps were obtained by differencing the time series, and errors for each coherent pixel ($\rho > 0.2$) in the displacement map were obtained by error propagation of estimated formal errors for each considered time series step.

GPS data were analyzed using all continuous stations in SE Spain spanning the 2006.00-2011.67 period. The processing of GPS data was done using two different strategies. All data sets were processed on a daily basis by using the GAMIT-GLOBK software packages to characterize the long-term and coseismic deformation patterns (Fig. 1). A 3 day period of high-rate data (1-Hz sampling) was processed by applying the instantaneous GPS positioning method to detect transient deformation associated to the earthquake occurrence (see Supplementary Material).

In the unloading mechanical model, we assumed 50 years (~1960-2010) of cumulative ΔCFF (slip-rake=36) resolved on the rupture fault-plane by crustal unloading due to 5 m/yr of groundwater table drop in an aquifer with 5% effective porosity. We approximate the aquifer shape as a rectangular unloading source shape (10x8 km^2 area, shown in Fig. S11a). The vertex of the aquifer is coincident with the point where the mapped fault trace changes in strike (La Tercia and Lorca segments of AMF), north of Lorca. At this location, the aquifer and mapped groundwater induced subsidence area are limited by the Guadalentin river, which runs approximately perpendicular to the Lorca-AMF segment (Fig. 1b and S11a). We assumed values for fault friction, c=0.5, and Skempton coefficient, B=0.6. Other models were also tested (see Supplementary Material). Files containing the displacement maps, fault-slip distribution model, and location of point sources for loading modelling can be obtained upon request to the corresponding author.

References

1. Dieterich, J. H. Modeling of rock friction: 1. Experimental results and constitutive equations. *J. Geophys. Res.* **84**, 2161–2168 (1979).
2. Marone, C. & Scholz, C. H. The depth of seismic faulting and the upper transition from stable to unstable slip regimes. *Geophys. Res. Lett.* **15**, 621–624 (1988).
3. Kaneko Y., Avouac, J.-P. & Lapusta, N. Towards inferring earthquake patterns from geodetic observations of interseismic coupling. *Nature Geosci.* **3**, 365–369 (2010).
4. Loveless, J. P. & Meade, B. J. Spatial correlation of interseismic coupling and coseismic rupture extent of the 2011 Mw=9.0 Tohoku-oki earthquake. *Geophys. Res. Lett.* **38**, L17306 (2011).
5. Simpson, D.W. Triggered earthquakes. *Ann. Revs. Earth Plan. Sci.* **14,** 21–42 (1986).
6. Seeber, L., Armbruster, J. G., Kim, W.-Y., Barstow, N. & Scharnberger C. The 1994 Cacoosing Valley earthquakes near Reading, Pennsylvania: A shallow rupture triggered by quarry unloading. *J. Geophys. Res.* **103**, 24505–24521 (1998).
7. McCarr, A., Simpson, D. & Seeber, L. Case histories of induced and triggered seismicity. In: International Handbook of earthquake and engineering seismology, **81A**. *In* Lee, W. H. K., Kanamori, H., Jennings P. C. & Kisslinger, C. (2002).
8. Fialko, Y., Sandwell, D., Simons, M. & Rosen, P. Three-dimensional deformation caused by the Bam, Iran, earthquake and the origin of shallow slip deficit. *Nature* **435**, 295–299 (2005).
9. Fielding, E.J., Lundgren, P.L., Bürgmann, R. & Funning, G.J. Shallow fault-zone dilatancy recovery after the 2003 Bam earthquake in Iran. *Nature* **458**, 64–68 (2009).
10. Stich, D., Serpelloni, E., Mancilla, F. & Morales, J. Kinematics of the Iberia-Maghreb plate contact from seismic moment tensors and GPS observations. *Tectonophysics* **426**, 295–317 (2006).
11. Masana, E., Martínez-Díaz, J.J., Hernández-Enrile, J.L. & Santanach, P. The Alhama de Murcia fault (SE Spain), a seismogenic fault in a diffuse plate boundary: seismotectonic implications for the Ibero-Magrebian region. *J. Geophys. Res.* **109**, B01301 (2004).
12. IGN, Informe del sismo de Lorca del 11 de Mayo de 2011 [in Spanish], http://www.ign.es/ign/resources/sismologia/Lorca.pdf (2011).
13. Lopez-Comino, J.A., Mancilla, F.d.L., Morales, J., & Stich, D. Rupture directivity of the 2011, Mw 5.2 Lorca earthquake (Spain). *Geophys. Res. Lett.* **39**, L03301 (2012).

14. González, P.J. & Fernández, J. Drought-driven transient aquifer compaction imaged using multitemporal satellite radar interferometry. *Geology* **39**, 551–554 (2011).
15. Okada, Y. Surface deformation due to shear and tensile faults in a half-space. *Bull. Seismol. Soc. Am.* **75,** 1135–1154, (1985).
16. González, P.J., Tiampo, K. F., Camacho, A. G. & Fernández, J. Shallow flank deformation at Cumbre Vieja volcano (Canary Islands): Implications on the stability of steep-sided volcano flanks at oceanic islands. *Earth Planet. Sci. Lett*. **297**, 545–557, (2010).
17. Frontera, T., et al. DInSAR coseismic deformation of the May 2011 Mw 5.1 Lorca earthquake (southeastern Spain). *Solid Earth* **3**, 111–119, (2012).
18. Martínez-Díaz, J.J. Stress field variations related to fault interaction in a reverse oblique-slip fault: the Alhama de Murcia fault, Betic Cordillera, Spain. *Tectonophysics* **356,** 291–305, (2002).
19. Hooper, A., et al. Increased capture of magma in the crust promoted by ice-cap retreat in Iceland. *Nature Geosci*. **4,** 783–786 (2011).
20. Heki, K. Snow load and seasonal variation of earthquake occurrence in Japan. *Earth Planet. Sci. Lett*. **207,** 159–164 (2003).
21. Klose, C. D. Geomechanical modeling of the nucleation process of Australia's 1989 M5.6 Newcastle earthquake. *Earth Planet. Sci. Lett.* **256,** 547–553 (2007).
22. Bettinelli, P., et al. Seasonal variations of seismicity and geodetic strain in the Himalaya induced by surface hydrology. *Earth Planet. Sci. Lett*. **266**, 332–344 (2008).
23. Cerón, J.C., and Pulido-Bosch, A. Groundwater problems resulting from CO_2 pollution and overexploitation in Alto Guadalentín aquifer (Murcia, Spain). *Environmental Geology* **28,** 223–228 (1996).
24. Boussinesq, J., *Application des Potentiels à l'Étude de l'Équilibre et du Mouvement des Solides Élastiques* (Reprint Paris: Blanchard, 1969, (1885)).
25. Rueda, J., Mezcua, J. & Garcia Blanco, R.M. Directivity effects of the May 11, 2011 Lorca (Spain) Mw=5.1 earthquake, S53B-2277, 2011 Fall Meeting, AGU, San Francisco, Calif., 5-9 Dec. (2011),
26. Marone, C., Scholz, C. & Bilham, R. On the mechanics of earthquake afterslip. *J. Geophys. Res.* **96**, 8441–8452 (1991).
27. Hetzel, R. & Hampel, A. Slip rate variations on normal faults during glacial-interglacial changes in surface loads. *Nature* **435**, 486–492 (2011).

28. Brothers, D., Kilb, D., Luttrell, K., Driscoll, N. & Kent, G. Loading of the San Andreas fault by flood-induced rupture of faults beneath the Salton Sea. *Nature Geosci.* **4**, 486–492 (2011).
29. Hampel, A., Hetzel, R., Maniatis, G. & Karow, T. Three-dimensional numerical modeling of slip rate variations on normal and thrust fault arrays during ice cap growth and melting. *J. Geophys. Res.* **114**, B08406 (2008).
30. González, P.J. & Fernández, J. Error estimation in multitemporal InSAR deformation time series, with application to Lanzarote, Canary Islands. *J. Geophys. Res.* **116**, B10404 (2011).

Supplementary Information is linked to the online version of the paper at www.nature.com/nature. The file contains Supplementary Text, Supplementary Tables S1-S2, Supplementary Figures S1-S13 with legends, and Supplementary References.

Acknowledgements

Our research was funded by an Ontario Early Researcher Award, the CSRN NSERC Strategic Network Grant, and the NSERC and Aon Benfield/ICLR IRC in Earthquake Hazard Assessment. PJG also acknowledges the Banting Postdoctoral Fellowship of the Government of Canada. Additional support was provided by the projects CGL2005-05500-C02, CGL2008-06426-C01-01/BTE, PCI2006-A7-0660, and AYA2010-17448; as well the Moncloa Campus of Excellence. Radar data from ESA CAT1:4460 and 6745 projects. GPS data from Meristemum, Red Activa de Murcia, and IGN networks. GMT software was used to create all figures. We are greatful to J.-P. Avouac, and two anonymous reviewers for their helpful comments. We thank to P. Bhattacharya, N. Cho, and F. Lorenzo-Martín for stimulating discussions, F. Luzón, and to J. Morales and A. Concha for sharing manuscripts before publication (ref. 13 and 17).

Authors’ contributions

PJG carried out the radar data analysis; dislocation, loading and pore-pressure diffusion models, and wrote the manuscript with the help of all co-authors. KFT and PJG carried out the CFF models. MP processed daily GPS data and computed the 2D strain-rate tensor. FC processed high-rate GPS data and analysed accelerometers frequency spectrum. JF and PJG designed the research.

Author information

The authors declare no competing financial interests.

Corresponding author

Correspondence to: Pablo J. González (pgonzal4@uwo.ca)

Figure 1 | Location and kinematics of the Lorca earthquake. a SE Spain seismicity (2000-2010), focal mechanisms (1970-2010), long-term GPS velocity (2006-2011, gray), and coseismic vectors (red). Major mapped faults are labelled. **b** Lorca city and Alto Guadalentin basin. IGN mainshock focal mechanisms (black), pre-shock (light-gray) and largest aftershock (dark-gray), and relocated seismic sequence[13]. Black stars are damages locations; Red lines faults[11]. Contour lines indicate 2 cm/yr InSAR subsidence due to groundwater pumping[14]. Blue rectangle: fault surface projection. **c** Groundwater depth evolution from different data sources (see Supplementary Information). **d** InSAR (triangles) and LOS projected GPS ground surface subsidence at LORC station.

Figure 2 | Ground deformation data and model. Descending LOS displacement maps and LORC station horizontal GPS vector (**a** and **c**) and distributed slip model predictions (**b** and **d**). **a** and **b** Data and model for track 008 (20110426-20110526). **c** and **d** Data and model for track 209 (20110510-20110609). Insets in **a** and **c** indicate LOS angle, positive values away from satellite. Blue rectangle: fault surface projection. Dashed lines are profile locations (**a-d**). **e** and **f** Observed and simulated data along two profiles, and local topography. 2σ data profiles based on standard deviation in a 1-km wide area normal to the profile direction.

Figure 3 | Fault slip and unloading stress change models. a Coseismic distributed fault slip model. **b** 50-years (~1960-2010) of cumulative ΔCFF (slip-rake=36) resolved on the rupture fault-plane by crustal unloading. **c** and **d** show fault-dip profiles ~2.5 km north of city (**c**) and in the Lorca (**d**) for the coseismic slip, and three cumulative unloading ΔCFF models with variable slip-rake (thrusting=blue, left-lateral=green and oblique=red with rake=36°). Background **c** shows depth percentage of the long-term crustal seismicity (2000-2010) located [www.ign.es] in SE Spain, under similar compressive regime, used to infer the depth of the upper frictional transition limit.

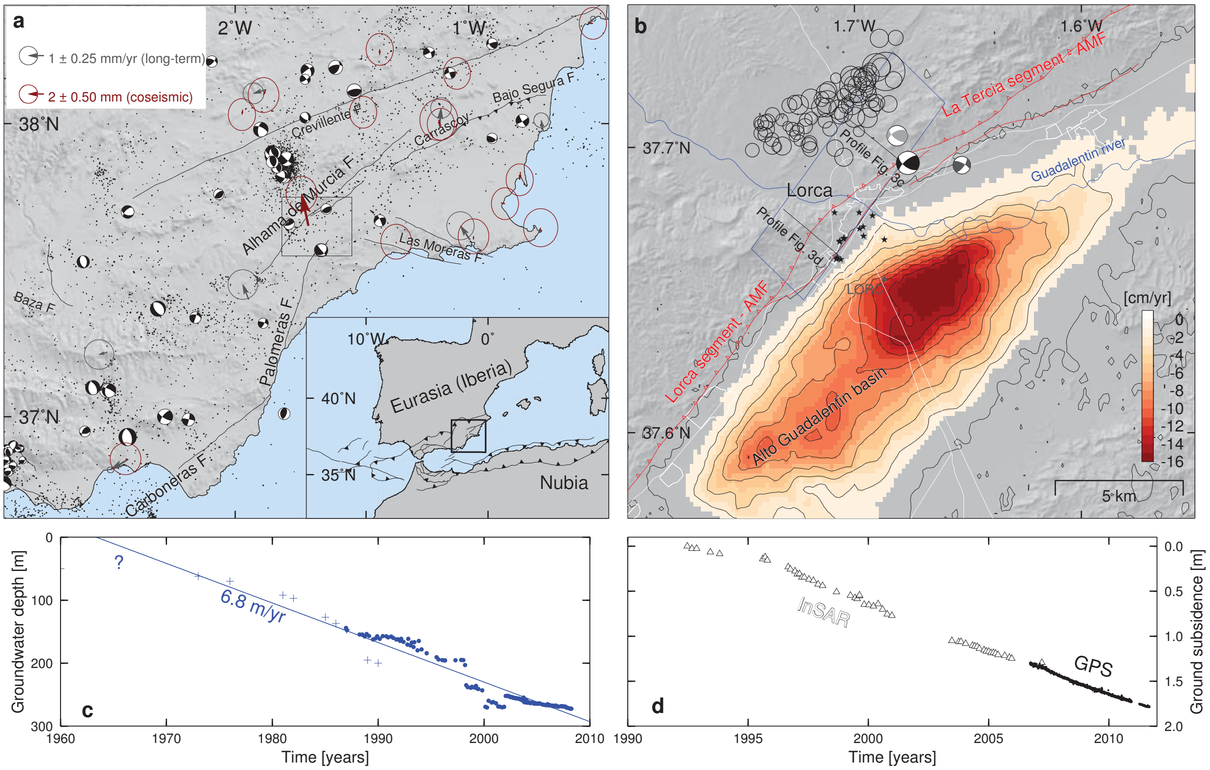
a
1 ± 0.25 mm/yr (long-term)
2 ± 0.50 mm (coseismic)
2°W
1°W
38°N
37°N
Crevillente F.
Bajo Segura F.
Carrascoy
Alhama de Murcia F.
Las Moreras F.
Baza F.
Palomeras F.
Carboneras F.
10°W
0°
40°N
35°N
Eurasia (Iberia)
Nubia
b
1.7°W
1.6°W
37.7°N
37.6°N
La Tercia segment - AMF
Lorca segment - AMF
Guadalentin river
Lorca
Profile Fig. 3c
Profile Fig. 3d
LORC
Alto Guadalentin basin
[cm/yr]
0
-2
-4
-6
-8
-10
-12
-14
-16
5 km
c
Groundwater depth [m]
0
100
200
300
?
6.8 m/yr
1960
1970
1980
1990
2000
2010
Time [years]
d
InSAR
GPS
Ground subsidence [m]
0.0
0.5
1.0
1.5
2.0
1990
1995
2000
2005
2010
Time [years]

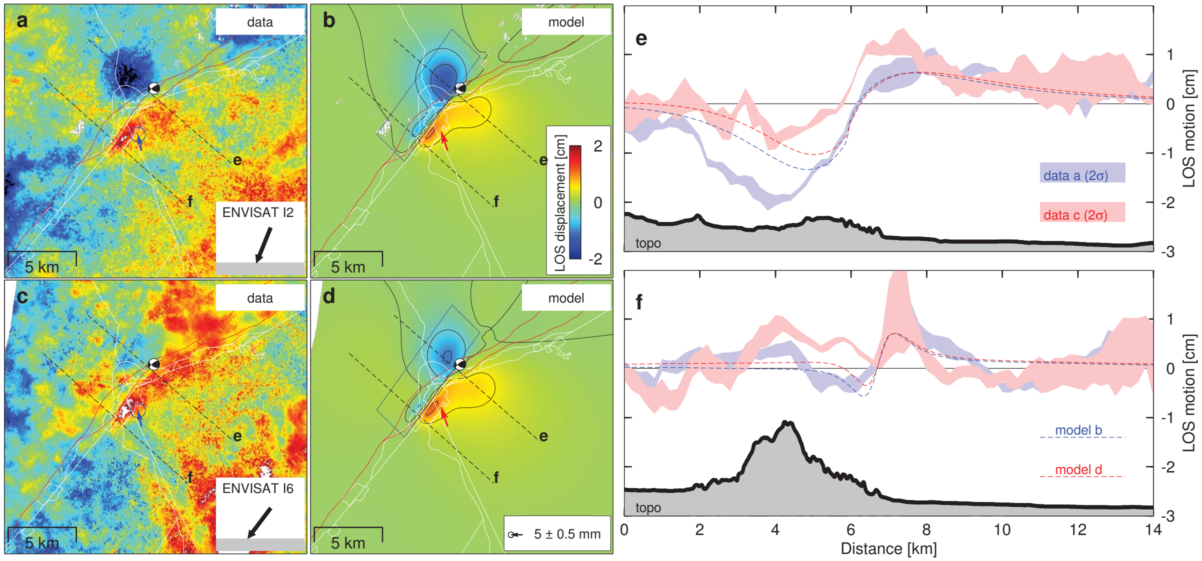
a
data
e
f
ENVISAT I2
5 km
b
model
e
f
LOS displacement [cm]
2
0
-2
5 km
c
data
e
f
ENVISAT I6
5 km
d
model
e
f
5 ± 0.5 mm
5 km
e
data a (2σ)
data c (2σ)
topo
LOS motion [cm]
1
0
-1
-2
-3
f
model b
model d
topo
LOS motion [cm]
1
0
-1
-2
-3
0
2
4
6
8
10
12
14
Distance [km]

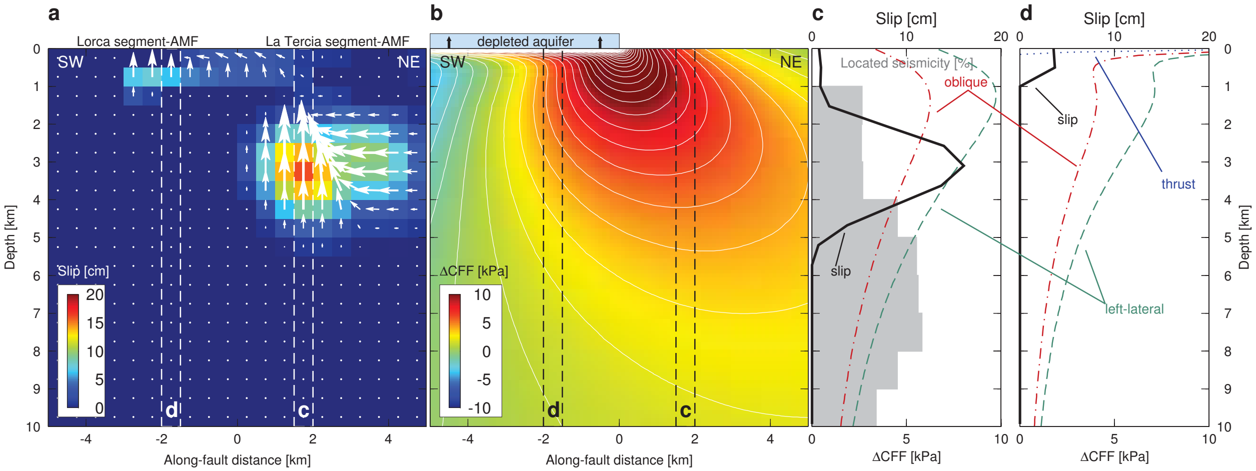
a
b
c
d
Lorca segment-AMF
La Tercia segment-AMF
SW
NE
Slip [cm]
20
15
10
5
0
Depth [km]
Along-fault distance [km]
depleted aquifer
ΔCFF [kPa]
10
5
0
-5
-10
Slip [cm]
Located seismicity [%]
oblique
slip
thrust
left-lateral
ΔCFF [kPa]
-4
-2
0
2
4
0
1
2
3
4
5
6
7
8
9
10